

# On the Effects of Modeling on the Sim-to-Real Transfer Gap in Twinning the POWDER Platform

Maxwell McManus<sup>1</sup>, Yuqing Cui<sup>1,2</sup>, Josh (Zhaoxi) Zhang<sup>1</sup>,  
Elizabeth Serena Bentley<sup>2</sup>, Michael Medley<sup>3</sup>, Nicholas Mastronarde<sup>1</sup>, Zhangyu Guan<sup>1</sup>  
<sup>1</sup>Dept. EE, University at Buffalo, USA; <sup>2</sup> U.S. AFRL; <sup>3</sup>SUNY Polytechnic Institute, USA  
Email: {memcmanu, yuqingcu, zhaoxizh, nmastron, guan}@buffalo.edu  
elizabeth.bentley.3@us.af.mil, michael.medley@sunypoly.edu

**Abstract**—Digital Twin (DT) technology is expected to play a pivotal role in NextG wireless systems. However, a key challenge remains in the evaluation of data-driven algorithms within DTs, particularly the transfer of learning from simulations to real-world environments. In this work, we investigate the sim-to-real gap in developing a digital twin for the NSF PAWR Platform, POWDER. We first develop a 3D model of the University of Utah campus, incorporating geographical measurements and all rooftop POWDER nodes. We then assess the accuracy of various path loss models used in training modeling and control policies, examining the impact of each model on sim-to-real link performance predictions. Finally, we discuss the lessons learned from model selection and simulation design, offering guidance for the implementation of DT-enabled wireless networks.

**Index Terms**—Modeling and Simulation, Sim-to-Real Gap, Digital Twin, Next-Generation Networks

## I. INTRODUCTION

The concept of Digital Twin (DT) has attracted substantial attention as an enabling technology next-generation (NextG) wireless communication systems [1]. Recent studies have demonstrated that integrating high-fidelity virtual wireless network models with their configurable real-world counterparts via DT can significantly enhance the performance of NextG networks. This improvement spans a wide range of applications, including computational offloading in mobile edge networks [2], UAV network configuration [3], and network resource management [4], among others.

However, the generalizations inherent in network simulations for DT often result in synthetic data that differs significantly from data collected over-the-air (OTA). This discrepancy further contributes to the sim-to-real gap, which refers to the performance deviation between simulated applications and their real-world deployment in OTA networking scenarios. For data-driven applications, an incomplete understanding of the sim-to-real gap can undermine model accuracy and lead to inefficient tuning of both model and simulation parameters, delaying the development of control policies.

In this work, using the POWDER platform as a case study, we take an initial step toward rigorous model selection evaluation within the DT design process for wireless networks.

This work was supported in part by the National Science Foundation (NSF) under Grant SWIFT-2229563 and the U.S. Air Force Research Laboratory under Contracts FA8750-21-F-1012 and FA8750-20-C-1021.

Distribution A. Approved for public release: Distribution Unlimited: AFRL-2024-4719 on 26 Aug 2024.

Specifically, we analyze the sim-to-real gap of a virtual model of the POWDER platform, generated using an open-source wireless network simulator, by examining two data-driven approaches: predictive modeling and network protocol optimization. We demonstrate the impact of model selection on the performance gap by comparing data-driven policies trained on synthetic data with those trained on real-world data collected from the POWDER platform.

The primary contributions of this work are as follows:

- We outline the virtualization process of the POWDER testbed as a reference for future DT design. The virtual testbed replicates the complete POWDER networking environment, including selected hardware and geographic specifics, and is implemented within the Universal Broadband Simulator (UBSim), an extensible open-source wireless network simulator [5].
- We leverage both physical and virtual POWDER testbeds to develop data-driven policies for two network control problems: predicting point-to-point link performance and optimizing protocols to maximize link quality-of-service (QoS). We then quantify the sim-to-real gap by comparing policies trained on synthetic data with those trained on over-the-air (OTA) data, and analyze the resulting performance differences between these two approaches.
- Based on our experimental findings, we explore the implications of applying a DT framework to the POWDER platform and provide recommendations for leveraging the platform in DT-enabled network design and control.

The remainder of the paper is organized as follows. Section II provides an overview of related works. In Section III, we detail the DT design process, including data collection and virtual model deployment. Section IV outlines the experimental approach used to benchmark the proposed DT system and Section V discusses the results of the experimental campaign. In Section VI, we share the lessons learned from the virtualization process. Finally, we draw the main conclusions in Section VII.

## II. RELATED WORK

Recent literature has seen a growing range of applications of DT technology in wireless systems. For example, the authors of [6] develop a high-fidelity DT of the city of Boston, incorporating existing cellular base station deployments. The

authors of [7] utilize the Colosseum platform to create a DT of the publicly available OTA indoor testbed Arena [8]. They detail the DT creation process and demonstrate that their framework achieves over 98% similarity in network performance, while also revealing the sim-to-real gap. In another study, [9] shows that the sim-to-real gap in a federated edge computing framework is minor, thanks to the high fidelity of trace-based channel modeling. Additionally, [10] explores sim-to-real transfer learning for device proximity estimation, where a deep learning policy is trained in simulation and fine-tuned in a real network, achieving 93% prediction accuracy.

These studies typically focus on testbeds with limited scale or controlled environments, leaving the study of the sim-to-real gap in long-range, outdoor scenarios relatively underexplored. Differently, in this work we examine the effects of model selection on the performance gap between DT simulations and real network performance. To the best of our knowledge, this work presents the first examination of the sim-to-real gap for data-driven modeling and control within community testbed platforms for advanced wireless research.

### III. VIRTUAL TESTBED DESIGN

We have divided the virtual testbed design process into two distinct steps. First, we conduct a geographical reconstruction of the testbed deployment within the simulation engine, incorporating 3D models of buildings, local topology, and node types. The second step involves behavioral modeling, where we define the parameters and functions for each modeled node type in the simulation engine. Before delving into these steps, we provide a brief overview of the POWDER platform, highlighting the key components essential for virtualization.

#### A. POWDER Platform: A Primer

POWDER [11] is a highly configurable, city-scale software-defined wireless networking testbed managed by the University of Utah in Salt Lake City, Utah. It features dozens of nodes deployed across a 14 km<sup>2</sup> area around Salt Lake City, including metropolitan, residential, and campus environments. The primary testbed is situated at the University of Utah campus and includes several node types: rooftop nodes, fixed (ground-level) endpoints, densely deployed nodes, mobile endpoints, and mMIMO nodes.

Given their geographic relevance, user popularity, and availability, we focus on the rooftop node deployments as central elements in the virtual framework design. There are eight rooftop nodes designated for use in the CBRS band, each equipped with two USRP X310 software-defined radios (SDRs) with UBX160 daughterboards and two USRP N310 SDRs with CBRS RF front-ends. All nodes are connected to a remote access and control framework based on Emulab, via various clusters located at the network edge.

#### B. Virtual Environment Construction

To construct a virtual replica of the POWDER deployment area, we utilized geographical information system (GIS) data obtained from the University of Utah Department of Geography and the U.S. Geological Survey National Map [12]. The collected data includes building height and elevation measurements, aerial photography of the University of Utah campus, and GPS coordinates for selected POWDER nodes.

The process of constructing the virtual system is illustrated in Fig. 1. On these maps, rooftop nodes are depicted as blue snowflake icons, while ground-level endpoints are shown as black antenna icons. Dense deployment nodes are marked with green antenna icons, and data centers are represented by black building icons, offering edge computing functionality.

We use the simulation engine UBSim [5] to model the behaviors of each selected node type. To import the POWDER geographical information into UBSim, we first generate best-fit axis-aligned bounding boxes (AABBs) using a map of buildings within the on-campus POWDER deployment area. These bounding boxes provide a general layout of the campus, allowing us to determine line-of-sight (LOS) or non-line-of-sight (NLOS) conditions between deployed nodes. As illustrated in Fig. 1(a), most buildings on the University of Utah campus are geometrically aligned and can be represented directly as AABBs, while some non-axis-aligned buildings require geometric adjustments. Building height data was supplied by the University of Utah. Next, we import elevation data for each building from the USGS National Map [12]. The elevation data is quantized into 15-meter intervals based on building groupings, as depicted by different colors in Fig. 1(b). The reference map is then rotated to align with the major axis used in UBSim, as shown in Fig. 1(c). Finally, Fig. 1(d)

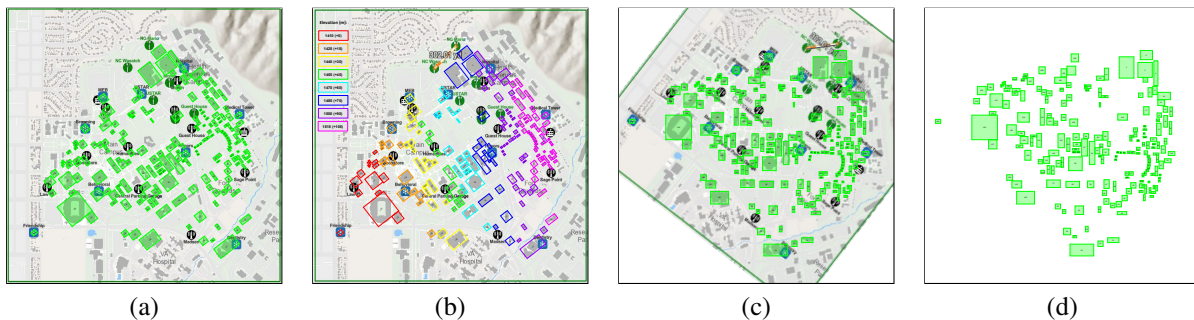


Fig. 1: Virtualization process of POWDER deployment environment: (a) generate best-fit bounding boxes for all buildings on the University of Utah campus using building dimension data; (b) assign building elevation based on topological data; (c) align bounding boxes with major axis; and (d) isolate AABB objects to import to UBSim.

displays the isolated AABB map objects, as imported into the Environment Definition API. In this work, we characterize the behaviors of select nodes based on both OTA measurements and standardized path loss models, as discussed below.

### C. OTA Measurement

The OTA measurements are performed using the Shout measurement framework [13], an open-source point-to-point measurement tool included by default in various POWDER profiles. The framework offers two default waveform options for OTA measurement: constant-waveform (CW) transmission and direct-sequence spread spectrum (DSSS) modulation. Given the interference levels observed during several measurement rounds, we have chosen to use the DSSS transmission method in our OTA measurements. DSSS is a spread-spectrum modulation technique which is used to provide both good signal quality in the presence of interference as well as data security by spreading transmitted information over a large bandwidth. To achieve this spreading, each modulated symbol of transmitted signal  $x$  with transmit power  $P_t$  is multiplied with a pseudo-random noise (PN) sequence, termed the spreading code  $c$ , resulting in a sequence of chips.

As detailed in Section III, our investigation focuses on communication between rooftop node deployments. To design these scenarios, we considered a comprehensive set of point-to-point link combinations among all available rooftop nodes, ensuring a robust experimental campaign. Data collection for each combination was carried out using the “*shout-long-2024*” profile, a customized configuration built around the Shout framework. This profile specifies transmission parameters, including PN sequence length, transmitter and receiver gain, measurement duration and repetition, and node selection, all organized into JSON files for straightforward user configuration.

Measurements were conducted opportunistically in the newly opened CBRS band, as outlined in Section I, by first sensing available spectrum resources to avoid interference. All measurements were performed within a center frequency range of 3550 to 3700 MHz, with minimal variation in frequency based on resource availability. It is worth noting that we have observed negligible differences in link performance within this frequency range.

We employ a round-robin transmission scheme to assess link performance between all rooftop-to-rooftop links. The scenario is set up by reserving a subset of rooftop nodes, as introduced in Section III, and configuring the selected profile at the time of reservation. Additionally, one compute node is reserved to act as the orchestrator, coordinating the automatic transmission and reception operations among the selected transceivers. To gather measurements, each selected rooftop node transmits a DSSS signal to all other selected rooftop nodes. This transmission is repeated 10 times, with average RSSI and SINR measurements collected at each receiving rooftop node. These measurements are then aggregated by the orchestrator and compiled into an HDF5 file for further processing.

Following this, the next rooftop node is designated as the transmitter, and the procedure is repeated with all other rooftop nodes serving as receivers. This process continues until all possible links have been evaluated. The rooftop nodes involved in this experiment include the Friendship Manor (FM), Brown-ing, Behavioral (BES), Honors, USTAR, Hospital, and Merrill Engineering Building (MEB) nodes. The Dentistry node was unavailable at the time of this experiment.

### D. Standardized Path Loss Models

Several standardized path loss models have been investigated to deploy in the simulated POWDER environment to accurately portray the RF conditions at the University of Utah propagation environment. These include the Friis free space path loss model, the ECC-33 model, and the Ericsson model. These models were chosen for their proven generalization capabilities and prediction accuracy in urban settings.

The free-space path loss model is commonly employed to estimate path loss based on frequency and distance, accounting for both line-of-sight (LOS) and non-line-of-sight (NLOS) conditions. Its widespread use in RF scenarios makes it a suitable choice for our analysis. The model is defined as  $PL(dB) = 32.45 + 20 \log_{10}(d) + 20 \log_{10}(f)$ , where  $d$  represents the link distance in kilometers and  $f$  denotes the transmission frequency in megahertz.

The ECC-33 model extends the Okumura and Hata path loss models to accommodate frequencies up to 8 GHz. It enhances the free-space model by incorporating gains related to base station and receiver heights. The model is formulated as  $PL(dB) = A_{fs} + A_{bm} - G_b - G_r$ , where  $A_{fs}$  is the free space attenuation,  $A_{bm}$  is the basic median path loss,  $G_b$  is the base station (BS) height gain factor, and  $G_r$  is the receiver height gain factor.

Finally, the Ericsson model builds upon the ECC-33 model by providing additional considerations for deployment environments. This extension allows for a more detailed representation of various environmental factors. The model is formulated as follows:

$$PL(dB) = a_0 + a_1 \log_{10}(d) + a_2 \log_{10}(h_b) + a_3 \log_{10}(h_b) \log_{10}(d) - 3.2(\log_{10}(11.75h_r)^2) + g(f) \quad (1)$$

where the frequency-dependent component  $g(f)$  is defined as  $g(f) = 44.49 \log_{10}(f) - 4.78(\log_{10}(f)^2)$ , and the coefficients  $a_0, a_1, a_2$ , and  $a_3$  are set for urban environments with values of 36.2, 30.2, 12, and 0.1, respectively<sup>1</sup>.

### E. Synthetic Dataset Generation

To generate the synthetic training data, we implement the propagation models detailed in Sec. III in the virtual POWDER environment deployed in UBSim to take advantage of its

<sup>1</sup>It is found in our experiments that these typical coefficients for urban, suburban, and rural environments do not fit the collected data due to the topographical variation of the physical environments. Therefore, we adopted  $a_0 = 26, a_1 = 10, a_2 = 12$ , and  $a_3 = 0.1$  to enhance model accuracy based on the collected data.

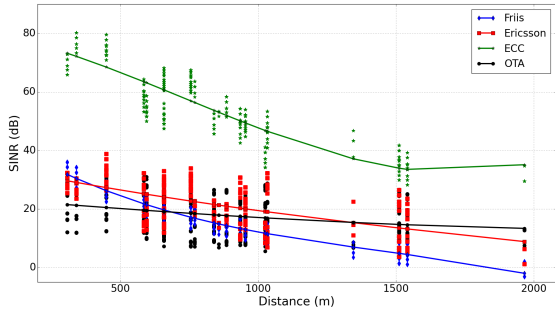


Fig. 2: Comparison of SINR values predicted by selected path loss models against values collected from OTA data (black).

3D geometry. The simulator was configured to replicate the experiment described earlier in this section, estimating SINR and BER for each transmitter-receiver pair. The goal of this process is to match the OTA data collected from the POWDER testbed, using link distance, transmitter and receiver height, spread spectrum processing gain, and LOS conditions from the virtual model. This results in three synthetic datasets, one for each propagation model considered.

A comparison of SINR values from each synthetic dataset against the OTA data is presented in Fig. 2, with a line of best fit included for each model. It can be seen that the Ericsson model (red) produces the most accurate SINR estimates, closely aligning with the OTA data. In contrast, the Friis model (blue) slightly overestimates path loss at greater distances, leading to lower-than-expected SINR values. The ECC model, however, underestimates path loss, resulting in overly optimistic SINR predictions. Although the ECC model tends to overestimate path loss, the gain terms related to transmitter and receiver height may fail to fully account for the steep elevation changes on the University of Utah campus, which are incorporated during the 3D modeling process.

#### IV. DATA-DRIVEN POLICY SELECTION

As discussed in Section I, this work aims to investigate the impact of the sim-to-real gap on data-driven control in wireless networks. To this end, we consider two representative networking tasks: predictive modeling of network behavior and network protocol optimization.

For both tasks, we leverage an Echo State Network (ESN) [14] for policy training. ESN is a type of recurrent neural network based on reservoir computing. As shown in Fig. 3 the ESN architecture is comprised of an input layer, a reservoir, and a trainable output layer. Define the ESN learning process with the number of observed variables  $N_V$ , the number of observed time steps,  $N_t$ , the number of collected data points,  $N_x$ , the size of the ESN reservoir  $N_h \times N_h$ , and the number of output variables,  $N_y$ . Then, the reservoir can be implemented as a series of neurons which define the internal state, represented as vector of activation outputs,  $\mathbf{h}(t) \in \mathbb{R}^{N_h}$ , to be a function of the ESN input. In most cases, the neuron model provides some leakage parameter,  $\alpha$ , by which the activation is determined by both  $\mathbf{h}(t)$  as well as previous state  $\mathbf{h}(t-1)$ , which improves learning capability of temporal features from

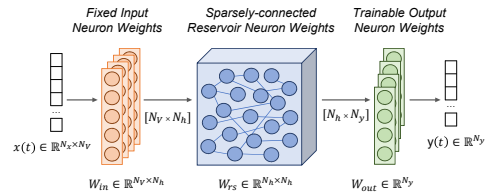


Fig. 3: ESN Architecture.

the input data. However, neither the input layer weights  $\mathbf{W}_{in} \in \mathbb{R}^{N_V \times N_h}$  nor the reservoir weights  $\mathbf{W}_{rs} \in \mathbb{R}^{N_h \times N_h}$  are trainable. The only trainable weights in the ESN are those of the output layer,  $\mathbf{W}_{out} \in \mathbb{R}^{N_h \times (1+N_V+N_h)}$ .

In order to apply the ESN to our tasks without significant temporal dependencies among inputs, a known output  $\mathbf{y}^*(t-1) \in \mathbb{R}^{N_y}$  can be applied in place of  $\mathbf{y}(t-1)$  to remove the recurrent relationship between  $\mathbf{h}(t)$  and  $\mathbf{y}(t)$ . This approach is termed *teacher forcing*, and can both accelerate the training process and adapt the network to more generalized learning tasks. For both tasks, we leverage teacher forcing to enable single-time-step evaluation since neither task relies on temporal features from the collected data. We use the PyESN library [15], and leverage a standard grid search method for hyperparameter selection.

*Task 1: Predictive Modeling:* The objective of this task is to estimate the signal-to-interference-plus-noise ratio (SINR) for a given link and protocol configuration. This task has been selected due to its ubiquity in existing literature, and is consistently leveraged as a basis for network deployment optimization, link capacity estimation in various spectrum bands, and optimizing spectrum coexistence and device co-location. For this task, we set  $N_V = 8$ , using variables such as TX-RX distance, TX node height, RX node height, and Gold code length, which has been one-hot encoded into five separate variables corresponding to the available options: 31-bit, 63-bit, 127-bit, 511-bit, and 2047-bit Gold code lengths. We set  $N_y = 1$ , representing the estimated SINR.

*Task 2: Protocol Optimization:* This task aims to predict the optimal PN code length for a given network topology and observed conditions. Due to the potential concerns for spectrum congestion while using the POWDER platform outlined in Sec. I, this task is intended to demonstrate how the use of a DT can improve communications performance through protocol configuration. Take advantage of the extensive parameterization of the Shout framework, the PN code can be selected to effectively balance the inherent tradeoff between resilience and throughput associated with DSSS PN code length selection outlined in Sec. III. For this task, we set  $N_V = 5$ , specifically using TX-RX distance, TX node height, RX node height, observed SINR, and observed BER. We set  $N_y = 5$ , corresponding to each of the available one-hot encoded Gold code lengths.

#### V. EXPERIMENTAL EVALUATION AND RESULTS

To illustrate the impact of the sim-to-real gap caused by the virtual POWDER testbed environment, we train a series of data-driven policies to address the tasks described in Sec. IV.

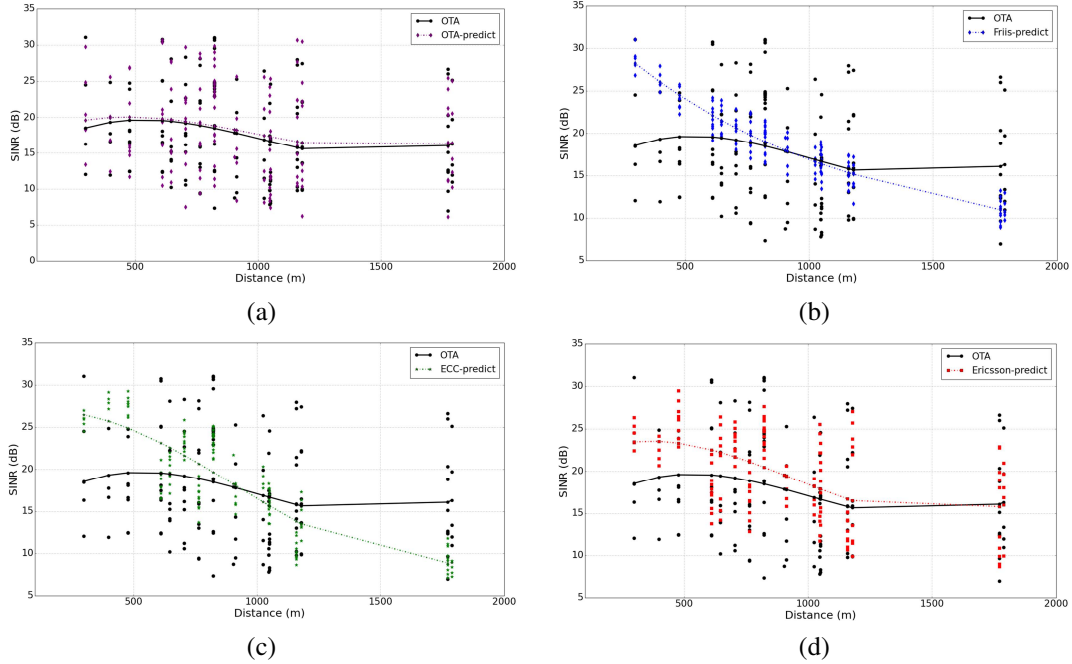


Fig. 4: Prediction of point-to-point SINR between rooftop nodes for the trained models: (a) ESN-1-OTA model (real-to-real), (b) ESN-1-Friis model (sim-to-real), (c) ESN-1-ECC model (sim-to-real), and (d) ESN-1-Ericsson model (sim-to-real).

We split the OTA dataset into training and evaluation sets, training a ground truth model for each task on the OTA training data. For each synthetic dataset, we train two models—one for each task. All models are then evaluated using the reserved OTA evaluation dataset. Finally, we compare the performance of the models trained on synthetic data with the OTA model for each task, highlighting the sim-to-real gap introduced by each propagation model.

To achieve this goal, we design and implement four ESN models to predict the optimal Gold code for each dataset. Each ESN model is named based on the task it was trained for and the data generation method used, following the convention “*ESN-#-model*”. We evaluate the performance of each model by comparing its outputs to the ground truth data, visualizing the results with best-fit lines to highlight the correlation between the outputs, and calculating the Mean Absolute Error (MAE) for each model.

The performance of models trained to predict point-to-point SINR (i.e. Task 1) are shown in Fig. 4. For each plot, the ground truth SINR results collected from the POWDER testbed are shown in black using a solid line, and each of the compared models are shown in color using a dashed line. The results clearly demonstrate the sim-to-real gap on the selected models. The ground truth model (i.e. trained on OTA data) is shown in Fig. 4(a). While the predicted data points show some variance between predicted and ground truth values, the model achieves a MAE of 2.011, and the trend of the prediction data is very similar to the ground truth dataset. The Friis model is shown in Fig. 4(b), and achieves a MAE of 4.957. This model does not incorporate any knowledge of transmitter or receiver height and thus poorly captures the trend of the

propagation environment. The greatest sim-to-real gap lies with the ECC model, shown in Fig. 4(c), which achieves a MAE of 5.643. The Ericsson model, shown in Fig. 4(d), offers poor performance at lower distances, but provides a good estimation of the trend of ground truth data at larger distances ( $\geq 1$  km), and achieves a MAE of 5.047. We can see that the predictive models based on ECC and Friis path loss models both seem to exaggerate the importance of distance on the resulting path loss in this environment.

The performance of models trained to predict optimal Gold code length (i.e. Task 2) are shown in Fig. 5 as a series of confusion matrices. For each plot, the optimal Gold code lengths estimated by each model are shown on the x-axis, and the ground truth labels are shown in the y-axis. The decimal ratio of correct predictions for each label are listed on the tile corresponding to that combination of predicted and ground truth labels. The performance of the “real-to-real” model (ESN-2-OTA) is shown in Fig. 5(a), which demonstrates perfect prediction accuracy for code lengths of 2047, 511, and 127, and very good accuracy for code lengths of 63 and 31. The performance of ESN-2-Friis is shown in Fig. 5(b), which shows very good prediction accuracy for length 2047 but poor accuracy for every other length. The results for ESN-2-ECC, shown in Fig. 5(c), demonstrate poor prediction accuracy for all labels, and indicate nearly random prediction of optimal code length. The ESN-2-Ericsson model performance in Fig. 5(d) is similar to that of the ESN-2-Friis model, in that both models predict optimal gold code length of 2047. While the selection of this code length will likely provide the best SINR, as discussed in Sec. III, this may not be the optimal choice in scenarios in which link quality is sufficient to support



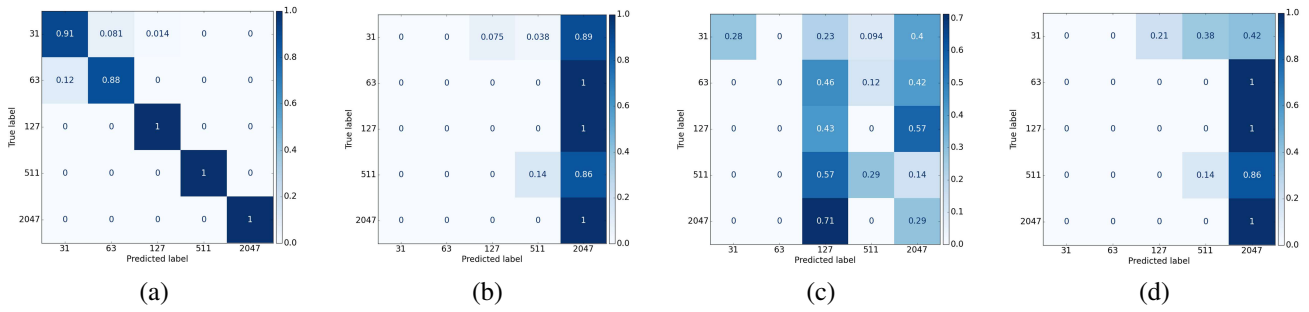


Fig. 5: Prediction of the optimal Gold code length on generated datasets: (a) ESN-2-OTA model (real-to-real), (b) ESN-2-Friis model (sim-to-real), (c) ESN-2-ECC model (sim-to-real), and (d) ESN-2-Ericsson model (sim-to-real).

higher data rates.

## VI. DISCUSSIONS

In this section, we summarize the key insights gained from our measurements on the POWDER platform as follows.

- *Spectrum Priority.* In the CBRS band, POWDER operates with the lowest-priority access, meaning incumbent users can cause significant interference during scheduled experiments. As a result, we had to repeat experiments over several days, leading to scheduling conflicts. The low transmit power also limited the communication range of the rooftop nodes. For future DT frameworks, we recommend incorporating automatic spectrum sharing based on historical data and a high-fidelity virtual environment to support offline experimentation when the RF environment is in use.

- *Hardware Configuration Monitoring.* During data collection, we discovered a mismatch between the antenna assignment in Shout and the current hardware configuration. While we were able to identify and correct this issue after analyzing the data and conducting manual measurements, such inconsistencies could pose a greater challenge for users running custom experimental profiles. We recommend that future DT systems include active monitoring and real-time status updates of all hardware components to automatically detect and resolve such discrepancies.

- *Channel Sounding.* We found the Shout framework’s documentation insufficient for extensive reconfiguration, leading to a time-consuming trial-and-error process. While general usage is well-documented, specifics on parameters are lacking. We recommend comprehensive documentation of all user-controllable parameters in future DT systems to facilitate efficient OTA data generation.

## VII. CONCLUSIONS

In this work, we investigated the sim-to-real gap in developing a digital twin for the NSF PAWR Platform, POWDER. We created a 3D model of the University of Utah campus, including geographical measurements and rooftop POWDER nodes, and assessed various path loss models for training and control policies. Our findings highlight the impact of model selection on sim-to-real link performance predictions and provide recommendations for improving DT-enabled wireless network design. In future work we will expand on this work by exploring additional node types, such as mobile nodes and

ground-level endpoints, and incorporating advanced simulation techniques like ray tracing.

## REFERENCES

- [1] M. McManus, Y. Cui, J. Hu, S. K. Moorthy, Z. Guan, N. Mastrorade, E. S. Bentley, and M. Medley, “Digital Twin-Enabled Domain Adaptation for Zero-Touch UAV Networks: Survey and Challenges,” *Computer Networks*, vol. 236, p. 110000, Nov. 2023.
- [2] W. Sun, H. Zhang, R. Wang, and Y. Zhang, “Reducing Offloading Latency for Digital Twin Edge Networks in 6G,” *IEEE Trans. on Vehicular Technology*, vol. 69, no. 10, pp. 12 240–12 251, Oct. 2020.
- [3] L. Lei, G. Shen, L. Zhang, and Z. Li, “Toward Intelligent Cooperation of UAV Swarms: When Machine Learning Meets Digital Twin,” *IEEE Network*, vol. 35, no. 1, pp. 386–392, Jan./Feb. 2021.
- [4] H. Wang, Y. Wu, G. Min, and W. Miao, “A Graph Neural Network-based Digital Twin for Network Slicing Management,” *IEEE Trans. on Industrial Informatics*, vol. 18, no. 2, pp. 1367–1376, Dec. 2020.
- [5] J. Hu, Z. Zhao, M. McManus, S. K. Moorthy, Y. Cui, N. Mastrorade, E. S. Bentley, M. Medley, and Z. Guan, “NeXT: Architecture, Prototyping and Measurement of a Software-Defined Testing Framework for Integrated RF Network Simulation, Experimentation and Optimization,” *Journal of Computer Communications*, Oct. 2023.
- [6] P. Testolina, M. Polese, P. Johari, and T. Melodia, “Boston Twin: the Boston Digital Twin for Ray-Tracing in 6G Networks,” in *ACM Multimedia Systems Conference*, Bari, Italy, Apr. 2024.
- [7] D. Villa, M. Tehrani-Moayyed, C. Robinson, L. Bonati, P. Johari, M. Polese, and T. Melodia, “Colosseum as a Digital Twin: Bridging Real-World Experimentation and Wireless Network Emulation,” *IEEE Trans. on Mobile Computing (Early Access)*, pp. 1–17, Jan. 2024.
- [8] L. Bertizzolo, L. Bonati, E. Demirors, A. Al-shawabka, S. D’Oro, F. Restuccia, and T. Melodia, “Arena: A 64-antenna SDR-based Ceiling Grid Testing Platform for Sub-6 GHz 5G-and-Beyond Radio Spectrum Research,” *Computer Networks*, vol. 181, p. 107436, Nov. 2020.
- [9] P. Pinyoanuntapong, T. Pothuneedi, R. Balakrishnan, M. Lee, C. Chen, and P. Wang, “Sim-to-Real Transfer in Multi-agent Reinforcement Networking for Federated Edge Computing,” in *IEEE/ACM Symposium on Edge Computing*, San Jose, CA, USA, Dec. 2021.
- [10] Y. Gao, G. Chi, G. Zhang, and Z. Yang, “Wi-Prox: Proximity Estimation of Non-Directly Connected Devices via Sim2Real Transfer Learning,” in *IEEE Global Communications Conference*, Kuala Lumpur, Malaysia, Dec. 2023.
- [11] J. Breen *et al.*, “Powder: Platform for Open Wireless Data-driven Experimental Research,” in *Proc. of International Workshop on Wireless Network Testbeds, Experimental evaluation and Characterization (WiNTECH)*, London, United Kingdom, Sept. 2020.
- [12] U. G. Survey, “National geologic map database project: Fort douglas, ut,” Accessed Mar. 8, 2023, 2020. [Online]. Available: <https://ngmdb.usgs.gov/topoview/viewer/#14/40.7652/-111.8492>
- [13] K. Webb, S. K. Kasera, N. Patwari, and J. K. V. der Merwe, “WiMatch: Wireless Resource Matchmaking,” in *IEEE Conference on Computer Communications Workshops*, Vancouver, BC, Canada, May 2021.
- [14] F. M. Bianchi, S. Scardapane, S. Løske, and R. Jenssen, “Reservoir Computing Approaches for Representation and Classification of Multivariate Time Series,” *IEEE Trans. on Neural Networks and Learning Systems*, vol. 32, no. 5, pp. 2169 – 2179, June 2021.
- [15] C. Korndörfer. pyESN: Echo State Networks in Python. [Online]. Available: <https://github.com/cknd/pyESN>